Cyclic Deformation Behavior and Buckling of Pipeline With Local Metal Loss in Response to Axial Seismic Loading

Masaki Mitsuya
e-mail: mitsuya@tokyo-gas.co.jp

Hiroyuki Motohashi
e-mail: motohasi@tokyo-gas.co.jp

Tokyo Gas Co., Ltd., Suehiro, Tsurumi,
Yokohama 230-0045, Japan

Buried pipelines may be corroded, despite the use of corrosion control measures such as protective coatings and cathodic protection, and buried pipelines may be deformed due to earthquakes. Therefore, it is necessary to ensure the integrity of such corroded pipelines against earthquakes. This study has developed a method to evaluate earthquake resistance of corroded pipelines subjected to seismic motions. Pipes were subjected to artificial local metal loss and axial cyclic loading tests to clarify their cyclic deformation behavior until buckling occurred under seismic motion. As the cyclic loading progressed, displacement shifted to the compression side due to the formation of a bulge. The pipe buckled after several cycles. To evaluate the earthquake resistance of different pipelines with varying degrees of local metal loss, a finite-element analysis method was developed that simulates cyclic deformation behavior. A combination of kinematic and isotropic hardening was used to model the material properties. The associated material parameters were obtained by small specimen tests that consisted of a monotonic tensile test and a low-cycle fatigue test under a specific strain amplitude. This method enabled the successful prediction of cyclic deformation behavior, including the number of cycles required for the buckling of pipes with varying degrees of metal loss. [DOI: 10.1115/1.4024451]

1 Introduction

Regardless of the efforts made to prevent corrosion, the possibility of corrosion cannot be ruled out over extended periods of time. Therefore, many studies have been conducted on pipelines to evaluate the effects of local metal loss on the remaining strength against internal pressure. Based on these studies, certain standards, including American Petroleum Institute/ASME Fitness-For-Service [1], have provided a criterion for the strength of pipelines with local metal loss due to corrosion in response to internal pressure.

In seismically active areas, the earthquake resistance of pipelines must be measured in addition to integrity against internal pressurization. Therefore, effects of monotonic bending moment [2] or monotonic axial compression [3] on pipelines with local metal loss have already been studied. In addition to the effects of these monotonic loadings, those of cyclic loading must be evaluated to show fitness for service of pipelines with local metal loss. While some recent studies have been conducted on aboveground pipes subjected to seismic ground motion [4–6], few studies have been conducted for buried pipelines [7]. Therefore, no appropriate evaluation method has been established for buried pipelines with local metal loss subjected to cyclic loading due to an earthquake.

Axial and bending loads on pipelines occur during an earthquake. This study focused on axial compressive loading. Although seismic loading on structures on the ground are generated from inertia forces, the generation mechanism of loading on buried pipelines is quite different from that of structures on the ground. Because seismic waves propagate in the ground, earthquakes generate a ground strain [8–10], which can mean nonuniform ground displacement up to about 0.5% [10]. When the direction of seismic displacement corresponds to the longitudinal direction of the pipeline, the axial compressive loading on the pipeline reaches its maximum value. Figure 1 shows the situation. The wavelength of the ground strain depends on the natural period of soil and is about 10–4100 m [10]. This ground strain generates a relative displacement between the soil and pipe. This relative displacement generates frictional force from the soil onto the pipe surface. Compressive loading is generated by integrating this frictional force in the axial direction.

With regard to the strength of a buried pipeline that is straight and uniform in the axial direction, the pipe strain ε_P is less than the ground strain ε_G in the elastic region, and the pipe strain ε_P is equal to the ground strain ε_G in the plastic region [8–10]. In other words, the ground strain ε_G can be used as the pipe strain ε_P when evaluating the earthquake resistance. Loading F in this condition can be expressed as $F = \sigma_P \cdot A = f(\varepsilon_P) \cdot A$. σ_P denotes the pipe stress, function f denotes the stress–strain relationship, and A denotes the cross-sectional area of the pipe. In this study, loading F was used as the applied loading on buried pipeline with local metal loss.

When the residual strength of a pipe with metal loss is greatly inferior to that of a pipe without metal loss, the pipe may have buckled. Otherwise, when the residual strength of the pipe is sufficient, the pipe has not buckled. However, even if the pipe does

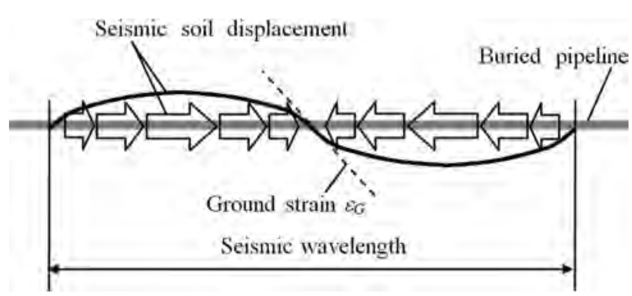

Fig. 1 Action of seismic wave on buried pipeline

Contributed by the Pressure Vessel and Piping Division of ASME for publication in the Journal of Pressure Vessel Technology. Manuscript received August 16, 2012; final manuscript received April 25, 2013; published online September 18, 2013. Assoc. Editor: Wolf Reinhardt.

not buckle, plastic deformation such as a bulge would accumulate and remain on the local metal loss after the first loading. Seismic loading would be repeatedly applied after this first loading. This cyclic loading would gradually promote plastic deformation in each cycle (this phenomenon is called ratcheting) and finally cause the pipe with local metal loss to buckle. Thus, because there is a buckling mode caused by cyclic loading and peculiar to pipes with local metal loss, it is essential to establish a method that evaluates the effect of cyclic loading on buried pipelines with local metal loss.

An equivalent number of cycles in a severe earthquake are described in the Japanese design code for gas pipelines. Five cycles should be assumed. Although this value is determined from a linear damage model of fatigue fracture and has no relationship with buckling by cyclic loading, this value was adopted as an approximation of the number of cycles to be considered in this study. In other words, this study targeted several cycles—i.e., up to 10 cycles.

In this study, axial cyclic loading experiments were carried out on line pipes subjected to seismic motion to clarify cyclic deformation behavior prior to buckling. The test pipes were machined so that each would have a different degree of local metal loss. A finite-element analysis method simulating cyclic deformation behavior, which applied kinematic and isotropic hardening components as material properties, was then developed.

2 Cyclic Deformation Behavior Observed in Cyclic Loading Experiment

2.1 Experimental Conditions and Procedure. Cyclic loading tests were conducted using steel pipes, hereafter referred to as pipe-A and pipe-B; their properties are listed in Table 1. Pipe-A has a diameter of 267.4 mm and wall thickness (t) of 7.6 mm; the diameter and wall thickness of pipe-B are 406.4 mm and 7.5 mm, respectively. Figure 2 illustrates the tensile properties the pipes.

A rectangular local metal loss was created by grinding the outer surface of the center of the pipe at a right angle to the longitudinal weld seam. As shown in Fig. 3, d, W, and L denote the depth, circumferential width, and longitudinal length of the local metal loss, respectively. All corners of the local metal loss were rounded with a radius of 1.0 mm. Table 2 displays the dimensions of the local metal losses taken from the cyclic loading experiments. Five experiments were conducted for pipe-A and one for pipe-B. Figure 3 illustrates the configuration of the experiments. The axial length of the test pipe was 4D, i.e., 1070 mm for pipe-A and 1630 mm for pipe-B.

The test load, axial displacement, and remote strain were measured during the experiments. The test load was measured using load cells installed between each hydraulic jack and the loading jig. The displacement was taken from the average of four displacement gages where the gage length of the displacement was 2D—i.e., 535 mm for pipe-A and 813 mm for pipe-B—and located at 90 deg intervals. The remote strain ε_R represents the average value of eight strain gages located 1D from the center and outside local metal loss. These eight strain gages were applied on the circumference at 90 deg intervals around the pipe.

Table 1 Properties of test pipes

	Pipe-A	Pipe-B
Diameter (mm)	267.4	406.4
Wall thickness (mm)	7.8	7.5
Grade	JIS STPG370 Sch30	JIS STPY400
Yield strength (MPa)	446	380
Tensile strength (MPa)	492	473
Yield-to-tensile ratio	0.91	0.80
Uniform elongation (%)	5.2	15.4
Formula	ERW	ERW

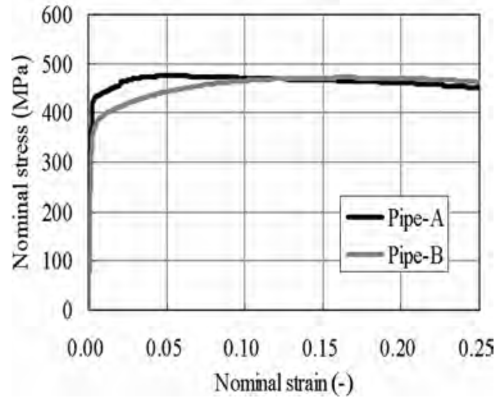

Fig. 2 Stress–strain relationship as revealed by the monotonic tensile specimen test

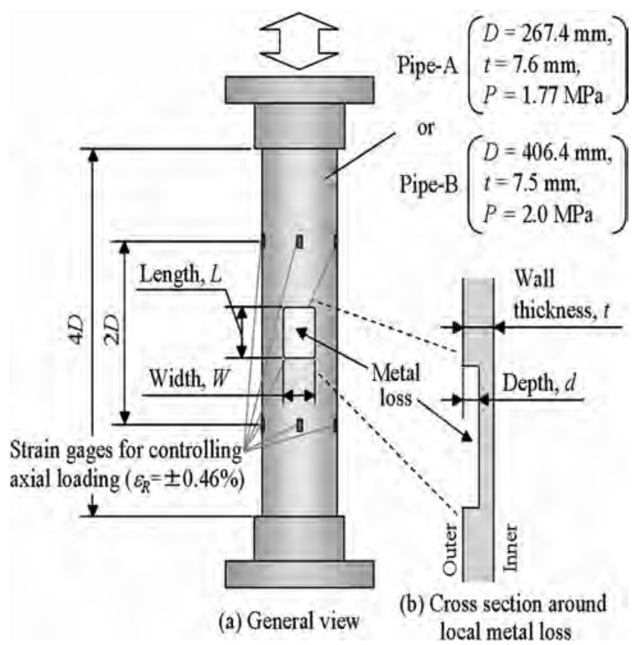

Fig. 3 Experimental setup

The cyclic loading tests were conducted according to the following procedure. Before a displacement was applied to the test pipe, the pipe was hydraulically pressurized to 1.77 MPa for pipe-A and 2.0 MPa for pipe-B. This internal pressure remained steady with no fluctuations during the experiment. A cyclic loading was then statically applied in the axial direction. The loading was controlled by the remote strain ε_R.

The loading direction was inverted when the absolute value of ε_R reached a specific value for both pipes to simulate the cyclic loading caused by seismic motion. As described previously, the seismic loading on a buried pipeline can be expressed as $F = \sigma_P{\cdot}A = f(\varepsilon_P){\cdot}A$. In cyclic loading, the stress–strain relationship f varies in each cycle, and the applied stress σ_P is not a constant value. Accordingly, the test was controlled by the pipe strain ε_P. ε_P originally denoted the axial strain of the pipe without metal loss. Therefore, the remote strain ε_R is the axial strain remote from the metal loss. When this remote strain ε_R reached the ground strain ε_G, this means that a load that simulates seismic loading was applied. When the remote strain ε_R could not reach the ground strain ε_G despite compressive displacement, this means that the pipe with local metal loss could not endure the seismic loading and buckled.

Table 2 List of experiments and analyses

Pipe	Case no.	Dimension of metal loss			Number of cycles until buckling	
		Depth d/t (%)	Width W (mm)	Length L (mm)	Experiment	Analysis
A	A1	15	100	100	20	14
	A2	15	320	320	4	3
	A3	20	100	200	13	13
	A4	20	200	100	4	4
	A5	30	100	100	7	6
B	B1	15	150	150	3	3

The strain amplitude threshold of the remote strain ε_R corresponding to the ground strain ε_G was set to 0.46%. This is almost the same as the maximum ground strain measured during severe earthquakes in Japan [10]. Previous studies [11,12] have confirmed that the strain rate due to ground deformation during an earthquake only slightly influences the tensile properties of steels; thus, the cyclic loading was applied statically.

2.2 Experimental Results. An example (case A5) of the shape of deformation is shown in Fig. 4. As cyclic loading progressed, compressive plastic strain accumulated and a bulge was formed in all test cases (Table 2). Figure 5 illustrates an example of the load–displacement relationship for case A5. The displacement shifted to the compression side cycle by cycle due to bulging. Finally, the displacement had increased before the remote strain surpassed –0.46% after several cycles as shown in Fig. 5. This phenomenon was defined as buckling in this study, e.g., case A5 underwent seven cycles until buckling. The number of cycles until buckling is summarized in Table 1.

Several comparisons indicate the effect of various parameters on time of buckling: A1 and A5 had the same length and width, but A5 (which had a deeper metal loss) experienced earlier buckling; A1 and A2 had the same depth, but A2 (which had a broader metal loss) experienced earlier buckling; and A3 and A4 had the same depth and planar dimensions, but A4 (which had a wider metal loss, meaning it was longer in the circumferential direction) experienced earlier buckling.

3 Hardening Model for Cyclic Loading

3.1 Selection of Hardening Model. Although deformation and buckling behavior has actually been observed in experiments, general experimental evaluation of the effects of local metal loss has not yet been possible. Although some studies have been conducted to examine [13,14] or simulate [15] cyclic loading on line pipes, a conclusive method for obtaining the buckling limit does not yet exist. Therefore, it is necessary to develop a finite-element analytical model to simulate cyclic deformation behavior prior to buckling and clarify the allowable dimensions of local metal loss in pipes subjected to ground motion.

Previous studies [16–18] have suggested that a constitutive model for cyclic loading is generally expressed in terms of kinematic and isotropic hardening components. (Figure 6 shows an example of compression–tension loading.) The blue arrow shows a translation of the yield surface center, corresponding to the kinematic hardening component, and the length of the orange arrows represents the radius of the yield surface, corresponding to the isotropic hardening component.

A kinematic hardening model is widely used as a constitutive model for simulating cyclic deformation behavior. Such a model describes the translation behavior of the center of a yield surface with a constant isotropic hardening component. The kinematic hardening model developed by Chaboche [19,20] is the most frequently implemented; however, it is unable to simulate cyclic deformation behavior accurately. Therefore, many alternative kinematic hardening models have been proposed in recent years

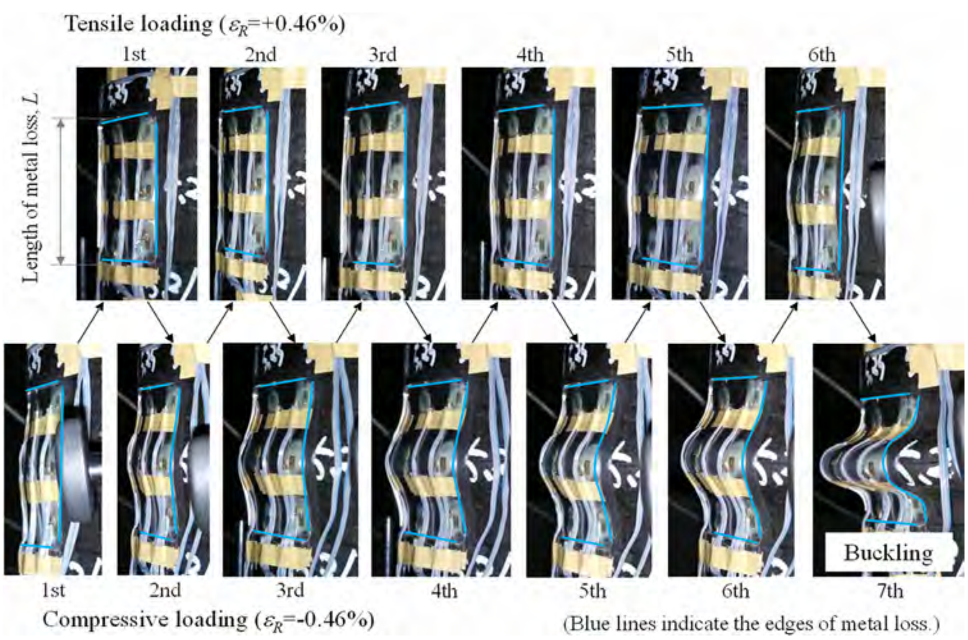

Fig. 4 Deformation shape revealed by experiment (case A5)

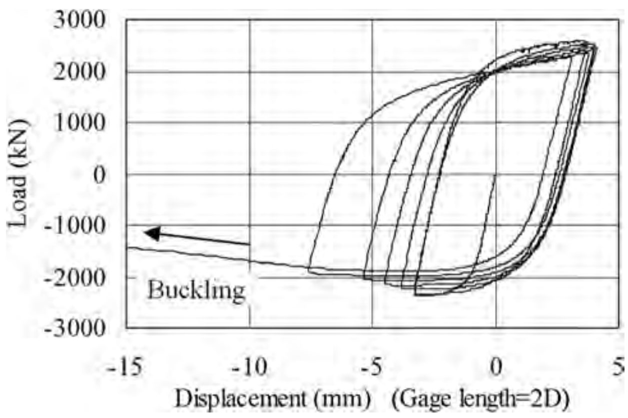

Fig. 5 Load–displacement relationship revealed by experiment (case A5)

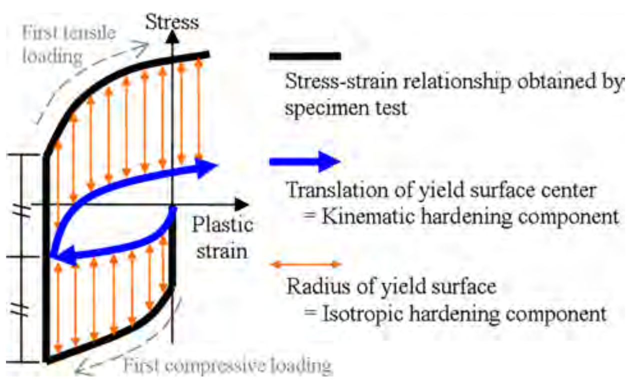

Fig. 6 Concept of kinematic and isotropic hardening

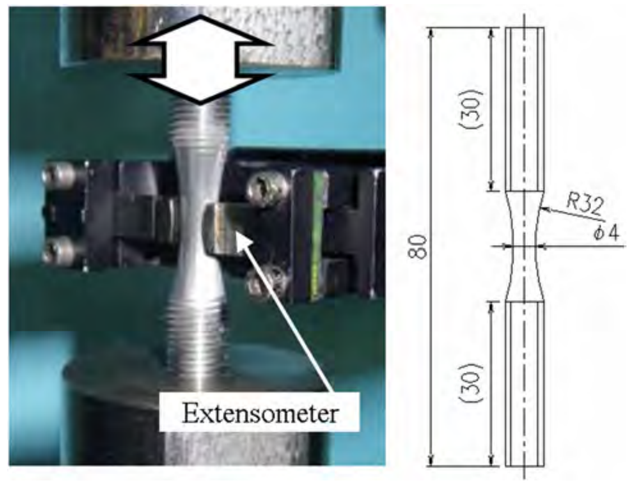

Fig. 7 Low-cycle fatigue test of the hourglass-shaped specimen

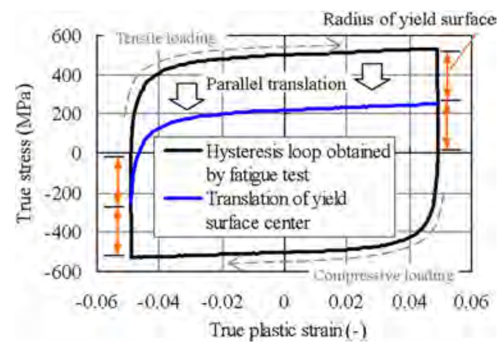

Fig. 8 Hysteresis loop at the middle of the lifetime obtained by the fatigue test (pipe-A, strain amp. = 5.1%)

[18,21–23]. Many studies have focused on two disadvantages of traditional kinematic hardening models such as Chaboche's model [19,20]: these models are not suitable for simulating history of stress amplitude under strain-controlled cyclic loading, similarly, not suitable for simulating history of strain amplitude under stress-controlled cyclic loading; and that they are not suitable for simulating deformation behavior under multiaxial loading.

When simulating deformation behavior of line pipes with local metal loss, as in the experiments in this study, these disadvantages are not severe. This is because the experiments focused on very low-cycle conditions: i.e., the changes in stress or strain amplitude during experiments were relatively small compared to those in previous studies aimed at developing a constitutive model. In addition, a macroscopically uniaxial deformation was observed in the experiments. However, one problem remains with the application of Chaboche's model to simulate the deformation behavior observed in the experiments.

The work-hardening behavior of a material immediately after the initial yielding, which is represented by the nonlinearity of the curve in the stress–strain relationship, is known to dominate its antibuckling performance [24–26]. In addition, a change in the work-hardening behavior from the first tension loading to subsequent loadings has been clearly observed in general carbon steels. For example, a Lüders plateau would be observed on the first loading but disappear on subsequent loadings. Most existing constitutive models for cyclic deformation have not incorporated this feature. Therefore, the development of a hardening model that can simulate a change in work-hardening behavior from the first loading to subsequent loadings is essential.

In this study, a combined kinematic–isotropic hardening model was used. In such models, the center of the yield surface moves in the stress space due to the kinematic hardening component and the yield surface range may expand or contract due to the isotropic component. The kinematic hardening component used was expressed by Chaboche's model [19,20] and the isotropic hardening component was expressed by a function of the cumulative equivalent plastic strain. Using this combined kinematic–isotropic hardening model, it was possible to simulate changes in the work-hardening behavior from the first tension loading to subsequent loadings.

3.2 Determination of Kinematic Hardening Component. The kinematic hardening component was abstracted from a low-cycle fatigue test under constant strain amplitude. The fatigue test specimen was sampled in the longitudinal direction of the pipe because the pipes used in the cyclic loading experiment macroscopically deformed in the longitudinal direction. The hourglass-shaped specimen shown in Fig. 7 was used to prevent buckling during compressive loading. The axial strain was calculated from the diametral strain, which was measured by an extensometer. The conversion was conducted based on ASTM-E606 [27].

A sample of a hysteresis loop, which represents the stress–strain relationship, is shown in Fig. 8. After several cycles, a symmetric loop such as that shown in Fig. 8 was observed. In the symmetric loop, the radii of the yield surface are the same on both the tension and compression sides. This conservation indicates a constant isotropic component in a cycle; thus, the parallel-translated blue line represents the translation of the yield surface center.

The kinematic hardening component was formulated according to the theory of Chaboche [19,20]. The component was described by the sum of α_1, α_2, α_3, and α_4 in this study. α_1, α_2, and α_3 were nonlinear functions, while α_4 was linear. The linear term is essential to represent work hardening in the large strain region.

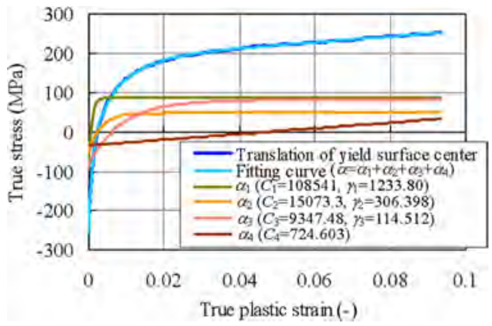

Fig. 9 Determination of kinematic hardening parameters from the fatigue test (pipe-A, strain amp. = 5.1%)

Integration of the backstress (center of yield surface) evolution laws over this uniaxial strain cycle, with an exact match for the first data of the blue line in Fig. 9, yields Eq. (1) [28].

$$\alpha_k = \frac{C_k}{\gamma_k}\left(1-\exp\left(-\gamma_k\cdot\varepsilon_p\right)\right)+\alpha_k^0\cdot\exp\left(-\gamma_k\cdot\varepsilon_p\right) \tag{1}$$

where α_k^0 denotes the k_{th} kinematic hardening component at the first data point as shown in Fig. 9 (initial value of the k_{th} kinematic hardening component). In the case of $\varepsilon_p = \Delta\varepsilon_p$, the value of the k_{th} kinematic hardening component (α_k^1) agrees with the negative of its initial value (α_k^1) because the original hysteresis loop shown in Fig. 8 is symmetrical about the origin.

$$\alpha_k^0 = -\frac{C_k}{\gamma_k}\left(\frac{1-\exp\left(-\gamma_k\cdot\Delta\varepsilon_p\right)}{1+\exp\left(-\gamma_k\cdot\Delta\varepsilon_p\right)}\right) \tag{2}$$

Equations (1) and (2) allow calibration of the parameters C_1, γ_1, C_2, γ_2, C_3, and γ_3. Similarly, C_4 for the linear kinematic hardening component was calibrated by Eqs. (3) and (4).

$$\alpha_k = C_k\cdot\varepsilon_p+\alpha_k^0 \tag{3}$$

$$\alpha_k^0 = -\frac{C_k}{2\cdot\Delta\varepsilon_p} \tag{4}$$

The calibrated material parameters are shown in Fig. 9; these were obtained from a low-cycle fatigue test conducted under a strain amplitude of 5.1%.

3.3 Effect of Strain Amplitude on Kinematic Hardening Component. The effect of the strain amplitude, which is a condition of the low-cycle fatigue test, was studied. Although the strain amplitude can be constant in a low-cycle fatigue test with a small specimen, it is not constant around the local metal loss on a pipe because plastic strain accumulates around the local metal loss and a bulge forms as a result of the cyclic loading. Therefore, kinematic hardening parameters were obtained by low-cycle fatigue tests under various strain amplitudes for both pipe-A and pipe-B. Figure 10(*a*) shows the obtained kinematic hardening components α $(=\alpha_1+\alpha_2+\alpha_3+\alpha_4)$ with α_k^0 being 0 in Eqs. (1) and (3), which indicates translation of the yield surface center under monotonic loading. Although each appears different at first glance, they do correspond after parallel translation on the vertical axis for each pipe (Fig. 10(*b*)).

The difference in Fig. 10(*a*) is interpreted to be due to an error in the definition of the linear limit of the hysteresis loop. As shown in Fig. 8, the hysteresis loops obtained by low cycle fatigue tests did not have distinct linear limits. Therefore, the obtained radius of yield surface must be accompanied with an error, as shown in Fig. 11. This error changes the center of the yield surface and generates a parallel translation of the kinematic hardening component, as shown in Fig. 11. In other words, various kinematic hardening components that are parallel to each other can be obtained from even one hysteresis loop that is focused on.

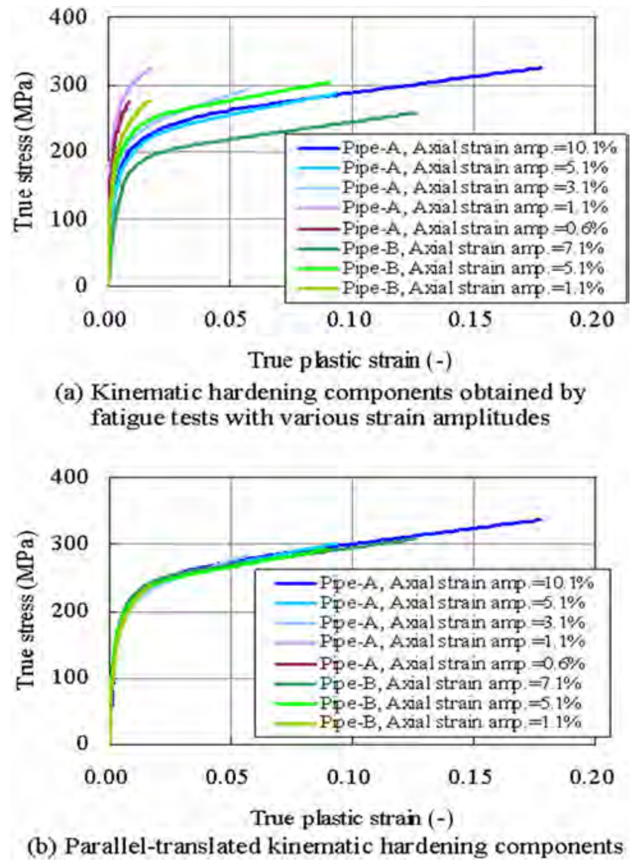

Fig. 10 Comparison of kinematic hardening components for various strain amplitudes

The effect of being parallel yet different was examined using a finite-element analysis. Two different materials, Mat. I and Mat. II were assumed (Fig. 12). The kinematic hardening parameters of these materials were configured so that the stress–strain curves were almost parallel to each other. Stress–strain curves obtained from a monotonic tensile test were configured to be the same, and the isotropic hardening components were determined as the differences.

A cyclic stress–strain relationship was calculated using one cubic element for both materials (Fig. 13). The overall responses obtained from both materials were similar, and the kinematic hardening components were parallel to each other. This indicates that the difference in the kinematic hardening components parallel to each other did not affect the cyclic deformation behavior—i.e., the kinematic hardening component obtained from the low-cycle fatigue test does not depend fundamentally on the strain amplitude.

Assuming that a low-cycle fatigue test under large amplitude is better than one under small amplitude because of the gradient of the kinematic hardening component in a region of high strain, work-hardening behavior cannot be obtained using only a small strain amplitude test. Therefore, the kinematic hardening component obtained from a low-cycle fatigue test conducted under an axial strain amplitude of 10.1% (Fig. 10) consists of the following components: $C_1=104409$, $\gamma_1=1911.18$, $C_2=46258.4$, $\gamma_2=407.484$, $C_3=4765.645$, $\gamma_3=66.0326$, and $C_4=471.563$; these were used to simulate the cyclic deformation behavior of pipe-A. As shown in Fig. 10(*b*), the kinematic hardening components of pipe-B, obtained by low-cycle fatigue tests, correspond to those of pipe-A, independent of strain amplitude. Therefore, the same components are used to simulate the cyclic deformation behavior for both pipes.

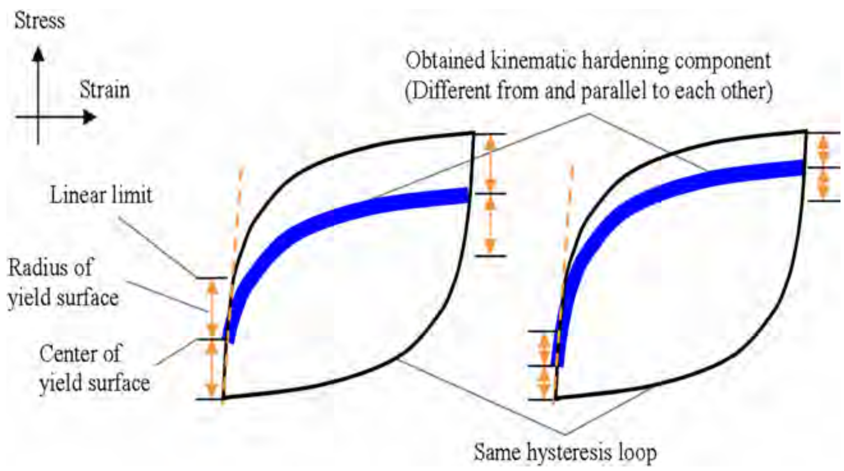

Fig. 11 Effect of error in the definition of the linear limit on obtained kinematic hardening component

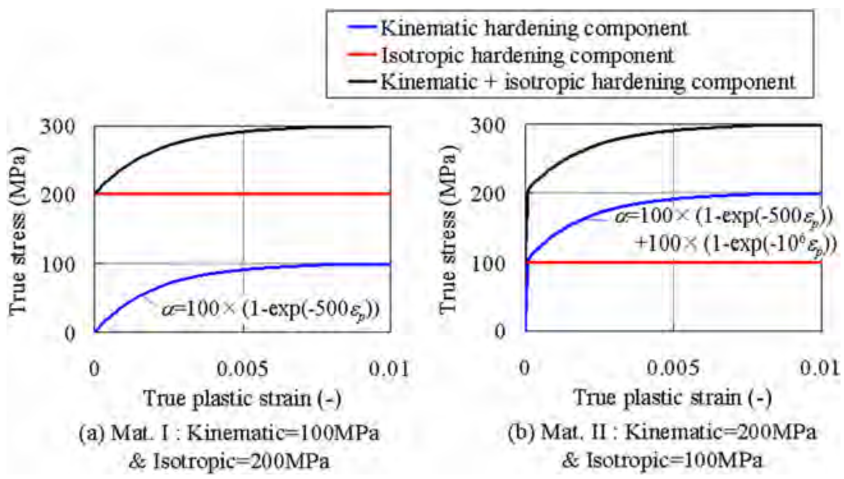

Fig. 12 Assumed cyclic hardening properties

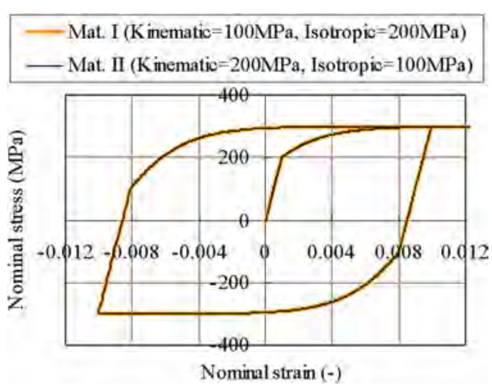

Fig. 13 Comparison of cyclic S-S relationship between parallel-translated kinematic hardening components

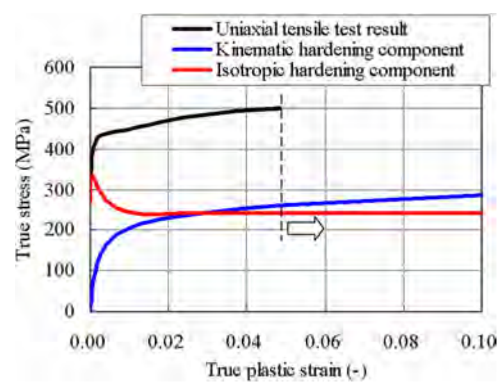

Fig. 14 Determination of isotropic hardening component (pipe-A)

3.4 Determination of Isotropic Hardening Component. The isotropic hardening component for both pipes was determined by subtracting the kinematic hardening component from the monotonic tensile result before uniform elongation. Figure 14 illustrates each component of pipe-A: the black line is the monotonic tensile result, the blue line the kinematic hardening component, and the red line the isotropic hardening component. Even though the isotropic hardening component decreases immediately after yielding, this phenomenon is derived from the Johnston–Gilman theory of dislocation [29].

The deformation behavior at the first loading is simulated accurately by determination of the isotropic hardening component from the differential of the monotonic tensile test result and the kinematic hardening component because the stress–strain relationship under monotonic loading is expressed by the sum of the kinematic and isotropic hardening components. However, a specific technique is required to obtain the relationship between true stress and true plastic strain after uniform elongation because of necking. Therefore, the isotropic hardening component before uniform elongation is used; the isotropic hardening after uniform elongation is assumed to be constant. Even though this assumption is applied, increase of true stress after uniform elongation under monotonic loading is represented because the kinematic hardening component increases monotonously, according to the linear term expressed in Eq. (3). The effect of this assumption on cyclic deformation behavior after the first loading is discussed in Sec. 3.5.

3.5 Validation of Material Definition. The material definition as described was validated by comparison between the results of a low-cycle fatigue test on a specimen and finite-element analysis using one cubic element. Abaqus/Standard version 6.11 [28] was used in the finite-element analysis.

The reproducibility of the stress–strain relationship in the first cycle was confirmed. The simulated stress–strain relationships are shown in Fig. 15(*a*); here, the stress–strain relationship was precisely simulated independently of strain amplitude. In particular, the roundness of the curve after the first tensile loading, which represents the work-hardening behavior and is dominant in the antibuckling performance, was simulated precisely. This was achieved due to the decrease in the isotropic hardening component immediately after yielding. Although the kinematic hardening component was determined from the result under a strain amplitude of 10.1% (Fig. 10(*b*)), the hysteresis loops under different strain amplitudes were also successfully simulated (Fig. 15(*a*)).

In the next step, the reproducibility after several cycles was confirmed. The stress–strain relationships at the fifth cycle are shown in Fig. 13(*b*). Similar to the first cycle, the roundness of the curves was precisely simulated, indicating that the material properties used in this analysis can simulate work-hardening behavior in each cycle.

However, this model cannot simulate the gradual change in stress amplitude sometimes observed in low-cycle fatigue tests under constant strain amplitude (Fig. 16(*a*)). As shown in Fig. 16(*b*), approximately constant stress amplitudes were calculated by finite-element analysis because the isotropic hardening component used in this analysis was approximately constant, except in the case of small strain (e.g., Fig. 10). The main difference between Figs. 14(*a*) and 14(*b*) is that the stress amplitude determined by finite-element analysis was approximately constant, in contrast to the stress amplitude determined by the specimen test. This means that the reproducibility possible by finite-element analysis decreases gradually as cyclic deformation progresses—i.e., reproducibility of the cyclic deformation behavior of pipes with local metal loss can be expected, where buckling occurs within several cycles.

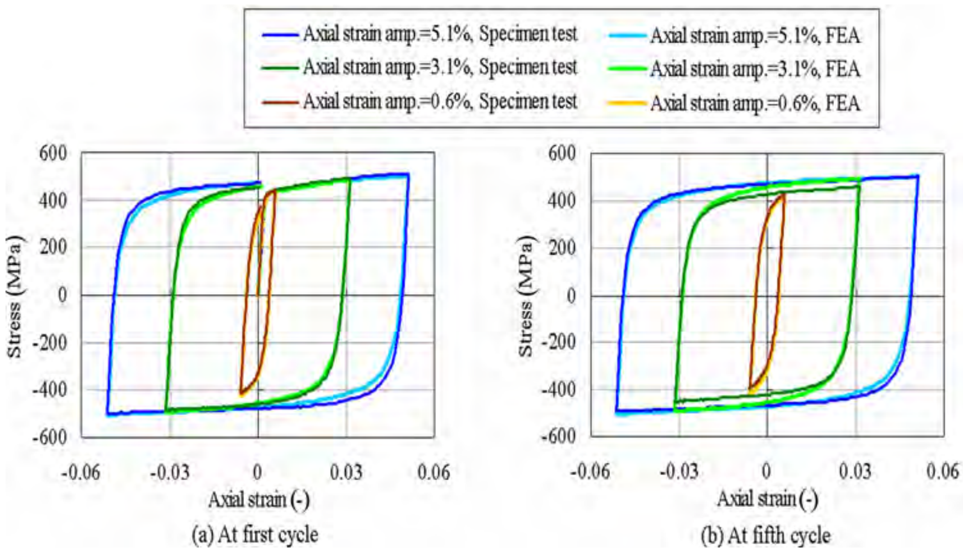

Fig. 15 Reproducibility of hysteresis loop (pipe-A)

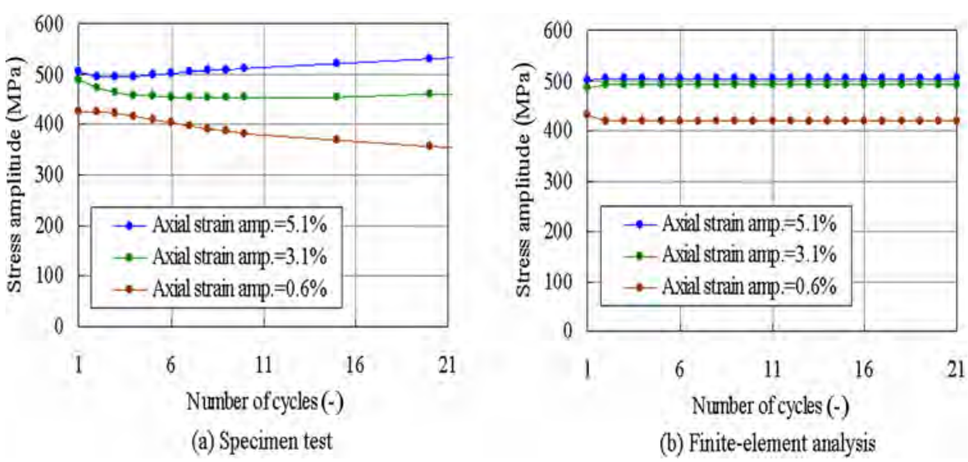

Fig. 16 Reproducibility of stress amplitude under constant strain amplitude (pipe-A)

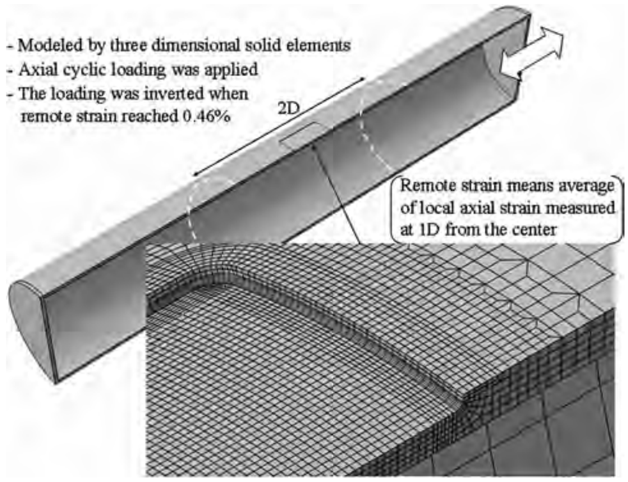

Fig. 17 Finite-element model (case A5)

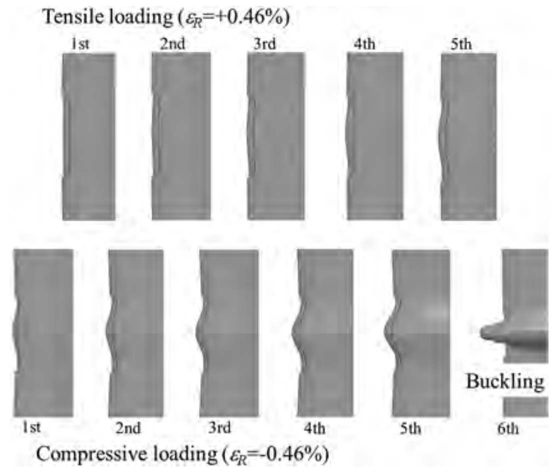

Fig. 18 Deformation shape by FEA (case A5)

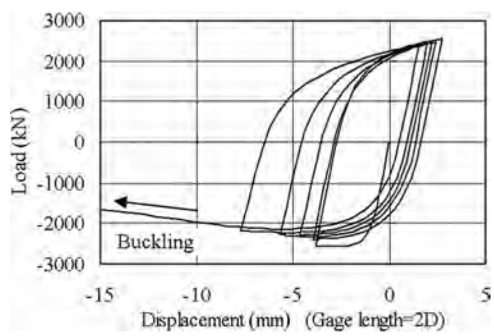

Fig. 19 Load–displacement relationship by FEA (case A5)

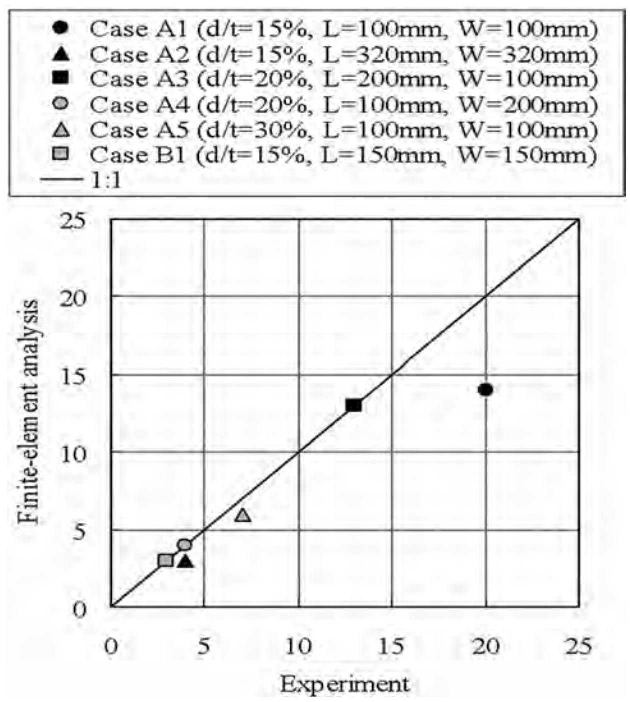

Fig. 20 Reproduction of number of cycles until buckling

4 Simulation of Cyclic Deformation Behavior by Finite-Element Analysis

4.1 Analytical Conditions. The cyclic deformation behavior of pipes with local metal loss was simulated by finite-element analysis; all of the cases shown in Table 2 were simulated. Figure 17 shows the finite-element mesh division in case A5. The local metal loss was modeled to have the same geometry as the experiment, as summarized in Table 2. Only half of the test pipe was modeled, due to its symmetrical nature. The finite-element model was built from three-dimensional, eight-node, reduced integrated solid elements. There were five divisions around the local metal loss in the wall thickness direction.

Abaqus/Standard version 6.11 [28] was used for the finite-element analysis. First, the internal pressure was applied and then the displacement was applied to the node corresponding to the end of the loading jig to simulate the experiment. As with the experiments, the loading direction was inverted when the remote strain reached 0.46%. For the purpose of simulating the deformation shape observed in the experiment, an eigenvalue buckling analysis representing a monotonic compression was conducted, and the result of this analysis was used as the initial imperfection. The maximum amplitude of the buckled shape obtained by the eigenvalue analysis was set to 0.1 mm.

As before, the kinematic and isotropic hardening components were defined as material properties. The kinematic hardening component obtained from low-cycle fatigue tests (blue line in Fig. 10(*b*)) was used for both pipe-A and pipe-B. The isotropic hardening component was determined by subtracting the kinematic hardening component from the monotonic tensile result (shown in Fig. 2) for both pipes. The components of pipe-A are shown in Fig. 14.

4.2 Analytical Results for Pipes. The finite-element analytical results were compared with the experiment to verify the applicability of the finite-element analytical method, including the definition of material, to evaluate the deformability of line pipes with local metal loss subjected to axial cyclic loading.

Figure 18 shows the deformation shape in the finite-element analysis; the local buckling that developed around the metal loss section was the same as that in the experiment, as shown in Fig. 4. Figure 19 shows the load–displacement relationship obtained from the finite-element analysis, indicating that the displacement shifted gradually to the compression side because of bulging and that the pipe buckled after several cycles.

The numbers of cycles until buckling was obtained by finite-element analysis are summarized in Table 2 and compared with these obtained experimentally. This comparison is shown in Fig. 20. All cases except case A1 were plotted along a 1:1 line. The discrepancy of case A1 can be explained by the reproducibility of the low-cycle fatigue test on an hourglass-shaped specimen. As shown in Fig. 16(*a*), the ratio of stress amplitude—i.e., the stress amplitude under a strain amplitude of 5.1% over a stress amplitude under a strain amplitude of 0.6%—was increased after several cycles in the experiment with the hourglass-shaped specimen. In the pipe experiment, the applied loading in each cycle was controlled by the remote strain ε_R, and its amplitude was 0.46%, which is approximate to 0.6%. In this experiment, because the strain amplitude in local metal loss would be greater than these values as cyclic plastic deformation was observed, as shown in Fig. 4, the material around metal loss would become harder after several cycles. In contrast, the cyclic material model used in the finite-element analysis could not display this hardening behavior, as shown in Fig. 16(*b*). Therefore, the hardening around metal loss after several cycles would not be represented, and the number of cycles until buckling in case A1 ($=20$) would be underestimated.

Other cases where buckling occurred within several cycles could be simulated precisely because the effects of insufficient reproducibility were small when early buckling occurred. The number of cycles until buckling could be simulated within several cycles; this indicates that the finite-element analytical method can be used to evaluate the integrity of pipelines with local metal loss against seismic motion in cases where buckling occurs within several cycles. The method described here allows for evaluation of the performance of pipelines subjected to severe seismic ground motion along with varying degrees of local metal loss.

5 Conclusions

In order to establish a method for evaluating the integrity of buried pipelines with local metal loss subjected to seismic motion, axial cyclic loading experiments for pipes and finite-element analyses were conducted. Based on this study, the following conclusions were obtained.

(1) As cyclic loading progressed, the displacement shifted to the compression side due to the formation of a bulge, resulting in the buckling of the pipe after several cycles.

(2) A finite-element analysis method was developed that simulates cyclic deformation behavior, including the number of cycles until buckling. A combination of kinematic and isotropic hardening components was used to model cyclic material properties. These components were obtained from small specimen tests that consisted of a monotonic tensile test and a low-cycle fatigue test under a specific strain amplitude. It was clarified that the difference in the strain amplitude on the low-cycle fatigue tests, which were used to obtain the kinematic hardening components, does not have an effect on cyclic deformation behavior.

Acknowledgment

The authors wish to thank Ms. Kimiko Keduka of Japan Open Systems Corporation for assistance with the FE analyses. Kobelco Research Institute and JFE Techno Research are gratefully acknowledged for their technical assistance in the experiments.

References

[1] ASME, 2007, *API 579-1/ASME FFS-1 Recommended Practice for Fitness-For-Service*, 2nd ed., The American Society of Mechanical Engineers, Washington, D.C.
[2] Shim, D. J., Choi, J. B., and Kim, Y. J., 2004, "Failure Strength Assessment of Pipes With Local Wall Thinning Under Combined Loading Based on Finite Element Analyses," ASME J. Pressure Vessel Technol., **126**, pp. 179–183.
[3] Chen, Q., Khoo, H. A., Cheng, R., and Zhou, J., 2010, "Remaining Local Buckling Resistance of Corroded Pipelines," Proceeding International Pipeline Conference, IPC2010-31512.
[4] Hasegawa, K., Miyazaki, K., and Nakamura, I., 2008, "Failure Mode and Failure Strengths for Wall Thinning Straight Pipes and Elbows Subjected to Seismic Loading," ASME J. Pressure Vessel Technol., **30**, p. 011404.
[5] Ohno, A., and Tahara, T., 2008, "Earthquake Resistant Design Code and Validation of Local Metal Loss Procedure Based on the Experimental Data Collected in Japan," Proceedings Pressure Vessels and Piping Conference, PVP2008-16845.
[6] Takahashi, K., Matsuo, K., Ando, K., and Urabe, Y., 2012, "Estimation of Low-cycle Fatigue Life of Elbow Pipes Considering the Multi-Axial Stress Effect," Proceedings Pressure Vessels and Piping Conference, PVP2012-78678.
[7] Hashimoto, Y., Hiroshi, Y., Hagiwara, N., and Oguchi, N., 2006, "Earthquake Resistance of Pipeline With Local Metal Loss Subjected to Cyclic Loading," Proceedings International Conference on Offshore Mechanics and Arctic Engineering, OMAE2006-92497.
[8] Shinozuka, M., and Koike, T., 1979, "Estimation of Structural Strain in Underground Lifeline Pipes," PVP-34, ASME, pp. 31–48.
[9] Toki, K., Fukumori, Y., Sako, M., and Tsubakimoto, T., 1983, "Recommended Practice for Earthquake Resistant Design of High Pressure Gas Pipelines," PVP-77, ASME, pp. 349–356.
[10] Japan Gas Association, 2000, Recommended Practice for Earthquake-Resistant Design of High Pressure Gas Pipeline (in Japanese).
[11] Minami, F., Morikawa, J., Ohshima, M., Toyoda, M., Konda, N., Arimochi, K., Ishikawa, N., Kubo, T., and Shimanuki, H., 1997, "Strength and Fracture Properties of Structural Steels Under Dynamic Loading," Proceedings International Conference on Offshore Mechanics and Arctic Engineering, Vol. 3, pp. 283–292.
[12] Yoshizaki, K., and Oguchi, N., 1998, "Effect of Strain Rate on Stress–Strain Properties of Gas Pipeline Steel," Proceedings of 10th Japan Earthquake Engineering Symposium, pp. 3171–3174 (in Japanese).
[13] Semiga, V., Tiku, S., Dinovitzer, A., Zhou, J., and Sen, M., 2008, "Development of a Pipeline Wrinkle Material Ultimate Limit State–Full Scale Modeling," Proceedings International Pipeline Conference, IPC2008-64620.
[14] Das, S., Cheng, J. J. R., and Murray, D. W., 2007, "Prediction of Fracture in Wrinkled Energy Pipelines Subjected to Cyclic Deformations," Int. J. Offshore Polar Eng., **17**(3), pp. 205–212. Available at: http://www.onepetro.org/mslib/servlet/onepetropreview?id=ISOPE-07-17-3-205
[15] Chen, X., Gao, B., and Chen, G., 2006, "Ratcheting Study of Pressurized Elbows Subjected to Reversed In-Plane Bending," ASME J. Pressure Vessel Technol., **128**, pp. 525–532.
[16] Bari, S., and Hassan, T., 2000, "Anatomy of Coupled Constitutive Models for Ratcheting Simulation," Int. J. Plast., **16**, pp. 381–409.
[17] Zakavi, S. J., Zehsaza, M., and Eslami, M. R., 2010, "The Ratchetting Behavior of Pressurized Plain Pipework Subjected to Cyclic Bending Moment With the Combined Hardening Model," Nucl. Eng. Des., **240**, pp. 726–737.
[18] Chaboche, J. L., 2008, "A Review of Some Plasticity and Viscoplasticity Constitutive Theories," Int. J. Plast., **24**, pp. 1642–1693.
[19] Chaboche, J. L., and Rousselier, G., 1983, "On the Plastic and Viscoplastic Constitutive Equations–Part I: Rules Development With Internal Variable Concept," ASME J. Pressure Vessel Technol., **105**, pp. 153–158.
[20] Lemaitre, J., and Chaboche, J. L., 1990, *Mechanics of Solid Mechanics*, Cambridge University, Cambridge, United Kingdom, pp. 161–241.
[21] Ohno, N., and Abdel-Karim, M., 2000, "Uniaxial Ratchetting of 316FR Steel at Room Temperature Part II: Constitutive Modeling and Simulation," J. Eng. Mater. Technol., **122**, pp. 35–41.
[22] Abdel-Karim, M., 2010, "An Extension for the Ohno-Wang Kinematic Hardening Rules to Incorporate Isotropic Hardening," Int. J. Pressure Vessels Piping, **87**(4), pp. 170–176.
[23] Takahashi, Y., and Tanaka, Y., "Development of Elastic-Plastic Constitutive Models for the Evaluation of Nuclear Piping Systems Under Severe Cyclic Loading," Proceedings Pressure Vessels and Piping Conference, PVP2012-78629.
[24] Gerard, G., 1956, "Compressive and Torsional Buckling of Thin Wall Cylinders in Yielded Region," NACA, TN-No. 3726.
[25] Suzuki, N., and Toyoda, M., 2002, "Critical Compressive Strain of Linepipes Related to Workhardening Parameters," Proceedings International Conference on Offshore Mechanics and Arctic Engineering, OMAE2002-28253.
[26] Yatabe, H., Fukuda, T., and Toyoda, M., 2004, "Effect of Material Stress-Strain Behavior and Pipe Geometry on the Deformability of the High-Grade Pipelines," ASME J. Offshore Mech. Arct. Eng., **126**, pp. 113–119.
[27] ASTM, 2004, E606-04e1, Standard Practice for Strain-Controlled Fatigue Testing.
[28] Simulia, 2011, Abaqus 6.11 Analysis User's Manual.
[29] Johnston, W. G., and Gilman, J. J., 1959, "Dislocation Velocities, Dislocation Densities, and Plastic Flow in Lithium Fluoride Crystals," J. Appl. Phys., **30**, pp. 129–144.